

# Controlled crystallization of Mn<sub>12</sub> single-molecule magnets by compressed CO<sub>2</sub> and its influence on the magnetization relaxation†

María Muntó,<sup>a</sup> Jordi Gómez-Segura,<sup>a</sup> Javier Campo,<sup>b</sup> Motohiro Nakano,<sup>c</sup> Nora Ventosa,<sup>a</sup> Daniel Ruiz-Molina\*<sup>a</sup> and Jaume Veciana\*<sup>a</sup>

Received 10th March 2006, Accepted 8th May 2006

First published as an Advance Article on the web 22nd May 2006

DOI: 10.1039/b603497g

Micro- and sub-micro particles of complex [Mn<sub>12</sub>O<sub>12</sub>(O<sub>2</sub>CC<sub>6</sub>H<sub>5</sub>)<sub>16</sub>(H<sub>2</sub>O)<sub>4</sub>] (**1**) with controlled size and polymorphism have been prepared by dense-gas crystallization techniques, showing a remarkable particle size influence on the magnetization relaxation rates.

## Introduction

Single-molecule magnets (SMMs) have a large spin ground state with appreciable magnetic anisotropy, resulting in a barrier for the spin reversal.<sup>1</sup> As a consequence, interesting magnetic properties such as out-of-phase ac magnetic susceptibility signals, magnetization hysteresis loops<sup>2</sup> and resonant magnetization tunnelling,<sup>3</sup> have been reported. Although the origin of such properties has been unequivocally attributed to individual molecules rather than to the existence of long range magnetic intermolecular interactions, they have been shown to be very dependent on structural and crystalline restrictions. For instance, previous works have shown the influence of dislocations on the resonant spin tunnelling of a crystal of Mn<sub>12</sub> clusters<sup>4</sup> or the existence of at least two different magnetization relaxation processes,<sup>5</sup> which are highly influenced by the network characteristics.<sup>6</sup> For these reasons, the preparation of crystalline samples of SMMs with controlled structural parameters, such as morphology, size and polymorphism, has become a challenge. If successful, this will give us a unique opportunity to study the influence of such structural parameters on the magnetization relaxation mechanisms.

Crystallization methods from conventional liquid solvents show very limited particle size and polymorphism control over the final particulate material. The reason for this is because these solvent-based processes are driven by temperature or system composition changes (temperature decrease, solvent evaporation, addition of anti-solvents, addition of salts, *etc.*), which are slowly and non-homogeneously transmitted in liquid media. In contrast, the solvation power of compressed fluids (CFs) in their liquid or supercritical state can be tuned by pressure changes, which propagate much more quickly and homogeneously than temperature and composition solvent

changes. Therefore, compressed solvents allow much greater control and tuning of the structural characteristics of the final material (size, porosity, polymorphic nature, morphology, *etc.*) than liquid solvents, and often lead to materials with unique physico-chemical characteristics unattainable by conventional processing methods.<sup>7–14</sup> For this reason, new crystallization procedures based on the use of CFs as solvent media have been shown to be very effective for the straightforward preparation of crystalline solids with micro-/nanoscopic particle size, smaller size dispersion and high polymorphic purity over the last two decades.<sup>15</sup> Most of these technologies have in common the use of CO<sub>2</sub> as a CF since it is non-toxic, non-flammable, cheap and easily recyclable. All these advantages have resulted in the appearance of different crystallization methods using CO<sub>2</sub> as a compressed fluid, which can be classified into four different groups according to the solvating behaviour of the CF in the process. So, the CF may behave as a solvent,<sup>16</sup> anti-solvent,<sup>17</sup> co-solvent,<sup>18</sup> or a solute.<sup>19</sup> As far as we know, these techniques have never been used before for the controlled crystallization of SMMs.

In this work we have prepared a set of crystalline samples of [Mn<sub>12</sub>O<sub>12</sub>(O<sub>2</sub>C<sub>6</sub>H<sub>5</sub>)<sub>16</sub>(H<sub>2</sub>O)<sub>4</sub>] (**1**), by the Gas Anti-Solvent crystallization (GAS) and the Aerosol Solvent Extraction System (ASES) techniques, which use compressed CO<sub>2</sub> as an anti-solvent.<sup>20,21</sup> In addition to the added value consisting of the preparation of SMM crystalline samples with control over morphology, size and polymorphism, magnetic characterization of these samples has revealed a significant influence on the magnetization relaxation rates.

## Experimental

### Materials

Complex **1** was synthesized as previously described.<sup>22</sup> CHCl<sub>3</sub> (purity 99.9%) was purchased from Romil Chemicals (Cambridge, UK) and used without further purification. Carbon dioxide (Purity > 99%) was kindly supplied by S.E. Carburos Metálicos (Barcelona, Spain).

### Methodology for the GAS crystallization

All GAS crystallization experiments of complex **1** were performed using an experimental set-up already described in

<sup>a</sup>Institut de Ciència de Materials de Barcelona (CSIC), Campus Universitari, 08193, Bellaterra, Catalonia, Spain.

E-mail: vecianaj@icmab.es; Fax: +34 93 580 57 29; Tel: +34 93 580 18 53

<sup>b</sup>Instituto de Ciencia de Materiales de Aragón, CSIC-Universidad de Zaragoza, CIPedro Cerbuna 12, 50009, Zaragoza, Spain.

Fax: +34 93 976 76 12 29; Tel: +34 34 976 76 27 42

<sup>c</sup>Department of Applied Chemistry, Graduate School of Engineering, Osaka University, 2-1 Yamada-oka, Suita, 565-0871, Japan.

E-mail: moto@ch.wani.osaka-u.ac.jp; Fax: +81 6 6879 4588;

Tel: +81 6 6879 4588

† This article is part of a themed issue on Molecular Magnetic Materials.

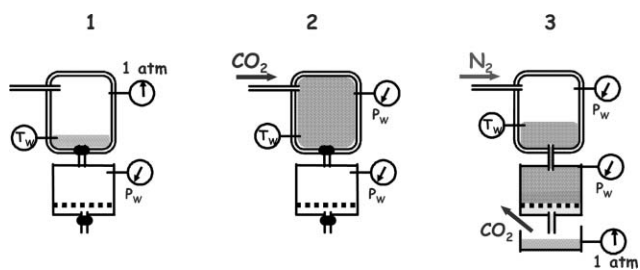


Fig. 1 Scheme of a GAS crystallization.

a previous work.<sup>23</sup> As schematized in Fig. 1, the methodology employed was as follows: a known volume,  $V_i$ , of a solution of complex **1** in  $\text{CHCl}_3$  with a supersaturation ratio of  $\beta_i = C/C_s = 0.9$ , where  $C$  stands for the actual concentration of complex **1** and  $C_s$  stands for the saturation limit at 298 K, was loaded into a 300 mL high pressure autoclave. The autoclave was then pressurized with  $\text{CO}_2$  to 10 MPa, while keeping the temperature constant at 298 K. Different values of  $\text{CO}_2$  system content,  $X_{\text{CO}_2}$ , could be attained by the loading of different amounts of  $V_i$ . Crystallization of complex **1** occurs during this process step. After leaving the system with mechanical agitation under the same conditions for 30 minutes to achieve complete homogenization of the mixture, the microparticles produced were filtered off. During the filtration step, the pressure inside the vessel and the filter was kept constant at 10 MPa by continuous addition of pressurized nitrogen gas from the top of the autoclave, in order to avoid the redissolution of the crystals. After filtration, the  $\text{N}_2$  flow was stopped, and the autoclave was depressurized to atmospheric pressure in order to withdraw the micronized powders.

### Methodology for the ASES crystallization

ASES crystallization experiments of complex **1** were performed using an experimental set-up already described in a previous work.<sup>23</sup> As schematized in Fig. 2, a constant flow of  $\text{CO}_2$  was continuously supplied inside a 300 mL high-pressure autoclave. The pressure inside the autoclave was kept constant at 10 MPa using a back pressure regulator valve. When constant values of temperature and pressure were achieved, pure  $\text{CHCl}_3$  was fed into the autoclave through an atomization nozzle (100  $\mu\text{m}$  diameter), at a constant flow, for several minutes after a constant  $X_{\text{CO}_2}$  was reached inside the vessel. The solvent flow was then stopped and a liquid solution of

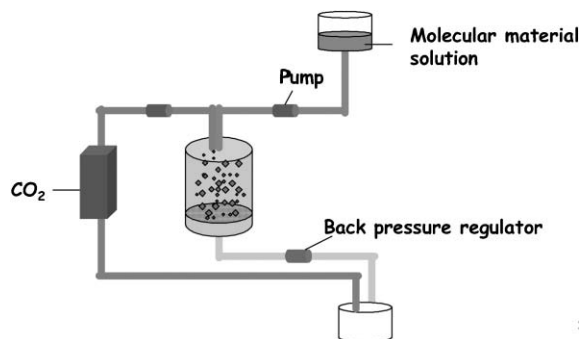


Fig. 2 Scheme of an ASES crystallization.

complex **1** in  $\text{CHCl}_3$  with a supersaturation ratio of  $\beta_i = 0.9$  was sprayed inside the autoclave at the same flow rate as the pure solvent.

The solid microparticles, produced through the ASES process during the spraying of the solution, were collected at 10 MPa on stainless steel filter housing and the mother liquid was depressurized after the back pressure valve. When all solution volume had been delivered, the  $\text{CO}_2$  flow was stopped, and the autoclave was depressurized to atmospheric pressure in order to withdraw the micronized materials.

### Sample characterization

Volume particle size distributions of samples were measured using a laser diffraction analyser (LS13.320, Beckman-Coulter, Fullerton, CA, USA), following ISO13320-1:1999. A sample (20 mg) of the micronized powder was suspended in 10 mL of special petroleum ether (Fluka, Germany) for its measurement.

The morphology of the samples was examined using a scanning electron microscope (SEM) (HITACHI S-570, Hitachi LTD., Tokyo, Japan); the samples were previously spread on a 9 mm silver film (FEDELCO S.L., Madrid, Spain) and coated with 10  $\text{\AA}$  of gold using a sputter coater (K550, Emitech, Ashford, UK).

X-Ray powder spectra were obtained by placing the sample into a 300 micron-diameter capillary and recording the spectra from  $2\theta = 2$  to  $60^\circ$  with a diffractometer (INEL CPS-120) working in Debye–Sherrer geometry. Alternating current (ac) magnetic susceptibility experiments were carried out on a Quantum Design SQUID magnetometer. Ac magnetic susceptibility curves were studied for samples of complex **1a–i** in the 1.8–10 K range with a 3.0 Oe ac oscillating field in the frequency range of 0.01–1400 Hz while the external magnetic field was held at zero. The magnetization relaxation times ( $\tau$ ) were obtained from the relationship  $\omega\tau = 1$  at the maxima of the  $\chi_M''$  vs. temperature curves. The  $\chi_M''$  peak positions were determined by fitting the  $\chi_M''$  vs. temperature data to one or two Lorentzian functions. Then the inverse of each peak position versus  $\tau$  was fitted, by least-squares procedures, to the Arrhenius law.

## Results and discussion

### Crystallization

Several successful crystallizations of complex **1** as a solid crystalline powder have been achieved by using the ASES and GAS anti-solvent techniques.  $\text{CHCl}_3$  was used as solvent whereas  $\text{CO}_2$  was used as anti-solvent. The reason for using  $\text{CHCl}_3$  as organic solvent lies in its miscibility with compressed  $\text{CO}_2$ ,<sup>24</sup> and its higher capability to dissolve complex **1** in relation to other common organic solvents such as hexanes or toluene (at 298 K measured solubility in  $\text{CHCl}_3$   $C_s(\mathbf{1}) = 3.3 \times 10^{-3} \text{ g ml}^{-1}$ ). In addition, we have experimentally observed that compressed  $\text{CO}_2$  behaves as an anti-solvent over solutions of complex **1** in  $\text{CHCl}_3$ , which is a prerequisite for the performance of both anti-solvent crystallization procedures. Several ASES and GAS crystallization experiments of SMM **1** from  $\text{CO}_2$  expanded chloroform solvent mixtures were carried

**Table 1** Particle size distribution of SMM **1** crystallized by GAS and ASES methods, from CO<sub>2</sub> expanded CHCl<sub>3</sub> mixtures, and by conventional diffusion crystallization using CH<sub>2</sub>Cl<sub>2</sub> as a solvent and hexane as anti-solvent

Exp	Crystallization method	Crystallization parameters			Particle size distribution <sup>a</sup>			
		X <sub>CO2</sub>	β <sub>i</sub>	T <sub>w</sub> /K	D[v,0.1]	D[v,0.5]	D[v,0.9]	U.I.
<b>1a</b>	Conventional diffusion	—	0.9	298	2	50	150	1
<b>1b</b>	GAS	0.5	0.9	298	5	30	65	8
<b>1c</b>	GAS	0.7	0.9	298	5	20	40	13
<b>1d</b>	GAS	0.8	0.9	298	5	15	35	15
<b>1e</b>	ASES	0.81	0.9	308	3.9	12	28	15
<b>1f</b>	ASES	0.84	0.9	308	2.5	6.5	14	19
<b>1g</b>	ASES	0.88	0.9	308	0.87	1.3	3.0	29
<b>1h</b>	ASES	0.92	0.9	308	0.89	1.1	1.5	66
<b>1i</b>	ASES	0.99	0.9	308	0.30	0.38	0.43	77

<sup>a</sup> Volumetric particle size distributions, measured by light scattering technique, are described by  $D[v,0.1]$ ,  $D[v,0.5]$  and  $D[v,0.9]$ , which are the particle diameters (μm) under which there are 10%, 50% and 90% of the total volume of the system, respectively.  $D[v,0.5]$  is the volume median particle diameter. Uniformity Index (U.I.), is defined as  $U.I. = [D[v,0.1]/D[v,0.9]] \times 100$ , and describes the polydispersity of the system.

out following the procedures described in the Experimental section. The crystallization operational parameters and the particle size characteristics achieved in these experiments are all summarized in Table 1.

### Structural characterization

**X-Ray powder diffraction.** From the study of the X-ray powder diffractograms of the different samples of complex **1** processed by the GAS and ASES methods, two main conclusions can be extracted: I) both crystallization techniques always produce particulate materials with high crystallinity and a very reproducible crystalline phase and II) such a reproducible crystallographic phase differs from the one obtained for the material crystallized by a conventional diffusion technique (sample **1a**), which in turn is in perfect agreement with the structure of **1** already published in the literature.<sup>22</sup> As an example, the powder X-ray diffractograms of samples **1b**, **1e** and sample **1a** (for comparison purposes) are shown in Fig. 3.

The obtaining of different crystallographic phases is a common situation for crystalline materials obtained by supercritical fluids. Indeed, in conventional anti-solvent diffusion crystallizations, the increase of the solution supersaturation

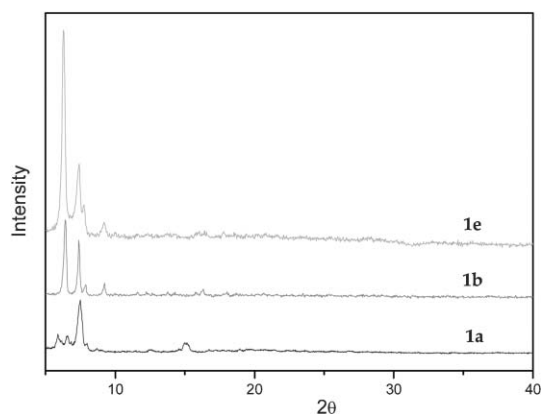


**Fig. 3** Powder X-ray diffraction patterns taken at room temperature for crystalline samples **1a**, conventionally crystallized, **1b**, produced by the GAS method, and **1e**, obtained by the ASES procedure.

takes place slowly, favouring the precipitation phenomena near equilibrium conditions, and therefore, the obtaining of the most thermodynamically stable form (whereas a given material shows polymorphism). In contrast, crystallization processes with CFs, driven by abrupt pressure or solvent composition changes, reach high supersaturation values ( $\beta$ ) in short periods of time. Therefore, crystallization phenomena take place far from the equilibrium conditions, favouring the obtaining of kinetically (metastable) forms. Unfortunately the small sizes of the resulting single crystals, obtained in GAS and ASES processes, of the new crystallographic phase of complex **1** prevent recording of the X-ray diffracting data with conventional diffraction techniques, preventing therefore the resolution of its structure.

It is important to emphasize here that the GAS and ASES processed crystalline samples are stable for long periods of time at room temperature. Such unusual stability, when compared with the high fragility of the crystals obtained by conventional diffusion techniques, may be explained by the absence of guest solvent molecules within the crystalline framework, as confirmed by elemental analysis and thermal studies.

**Particle size distribution.** All the crystalline powders obtained by the GAS or ASES procedures exhibit a median particle size smaller than those produced by conventional diffusion crystallization techniques as well as a higher uniformity index. As shown in Table 1, the particle size distribution of crystalline samples resulting from GAS and ASES experiments can be tuned by varying the operational process parameters. Although in both techniques the crystallization driving force is the anti-solvent power of CO<sub>2</sub> over the solution of complex **1** in CHCl<sub>3</sub>, smaller particles with a narrower particle size distribution were achieved by the ASES crystallization procedure. Indeed, whereas in GAS crystallization the diffusion of the CO<sub>2</sub>, and as a consequence the induction of precipitation, is improved by vigorous stirring, in the ASES technique the promotion of the CO<sub>2</sub> diffusion in the solute bearing solution is more effectively enhanced by formation of an aerosol of the solution before the CO<sub>2</sub> antisolvent induces precipitation.<sup>17</sup> By varying only the CO<sub>2</sub> content of the system, using both dense gas anti-solvent

crystallization techniques, we were able to obtain samples of SMM **1** with a  $D[v,0.5]$  ranging from 30 to 0.38  $\mu\text{m}$ , and with a U.I. varying from 8 to 77. The higher is  $X_{\text{CO}_2}$ , the higher is the maximum supersaturation attained in the solution enhancing nucleation over crystal growth, and therefore resulting in smaller particles with a narrower size distribution.

**Scanning electron microscopy.** As can be seen in Fig. 4, the scanning electron microscopy (SEM) image of a sample of complex **1** obtained by a standard diffusion of *n*-hexane into  $\text{CH}_2\text{Cl}_2$  (sample **1a**) reveals a broad distribution of sizes and morphologies, showing the crystals have several defects and imperfections. Such a distribution is even favoured in some cases by the loss of interstitial crystallization solvent molecules, and the subsequent fragmentation of the original crystalline material.

In contrast, the SEM images of SMM **1** processed either by GAS or ASES crystallization methods reveal the formation of crystals with considerably improved size uniformity and a smaller volume median particle size diameter. Representative examples of samples obtained by both GAS (sample **1b**) and ASES method (samples **1f** and **1h**) are shown in Fig. 4. The SEM image of the crystalline sample **1a** obtained by a classical diffusion process is also shown for comparison purposes. As can be seen, using the GAS anti-solvent technique, micron-sized particles were produced whereas by the ASES crystallization route sub-micron particle were achieved with a higher uniformity index (U.I. = 8–77) than that achieved by conventional diffusion crystallization (U.I. = 1). Finally, the SEM images shown in Fig. 5 are representative of the potential of these crystallization techniques to tune the particle size of complex **1**, by only modifying the  $X_{\text{CO}_2}$  operational parameter in ASES crystallization experiments. Indeed, crystals obtained in experiment **1e** performed at  $X_{\text{CO}_2} = 0.8$  are one order of magnitude larger and more polydisperse ( $D[v,0.5] = 12$ ,

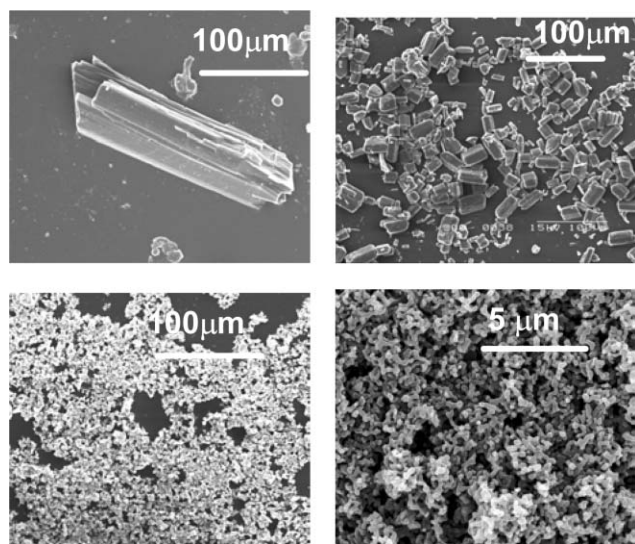


**Fig. 4** SEM images taken on sample **1a** (upper left) obtained by a conventional crystallization, sample **1b** (upper right) prepared by a GAS crystallization technique, and samples **1f** (lower left) and **1h** (lower right) prepared by ASES crystallization.

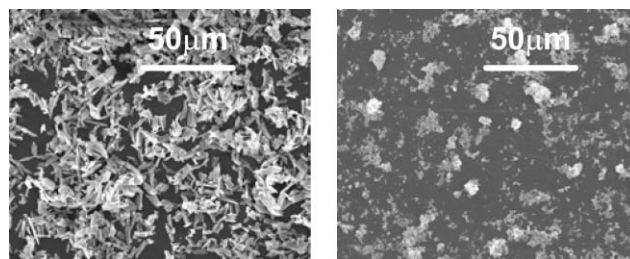


**Fig. 5** SEM images taken on crystalline SMM **1** obtained by ASES at  $X_{\text{CO}_2} = 0.81$ , sample **1e** (left), and at  $X_{\text{CO}_2} = 0.99$ , sample **1i** (right).

U.I. = 15) than those collected in experiment **1i** ( $D[v,0.5] = 0.38$ , U.I. = 77), performed with exactly the same operational parameters but higher  $X_{\text{CO}_2} = 0.99$ .

### Magnetic properties

Magnetic characterization of samples **1a** (diffusion), **1b** (GAS) and **1e** (ASES) reveals two peaks in the out-of-phase ac signal ( $\chi_M''$ ) of each sample, associated with the presence of at least two different magnetization relaxation mechanisms.<sup>5</sup> The existence of both out-of-phase peaks is not new and has already been described for several other  $\text{Mn}_{12}$  single-molecule magnets. However, a detailed study reveals unexpected differences in the resulting effective interconversion energy barriers. In the case of the slowest relaxation process, the effective energy barriers ( $U_{\text{eff}}$ ) were 65.1 K, 66.7 K and 65.4 K for samples **1a**, **1b** and **1e**, respectively, whereas for the fastest relaxation mechanism they were 38.4 K, 36.1 K and 37.9 K for samples **1a**, **1b** and **1e**, respectively (Table 2).

Due to the differences previously observed for the energy barrier and to rule out the possible influence of polymorphism, the magnetic properties of samples **1b–1i** were measured and analyzed, since all these samples exhibit the same crystallographic phase. First, ac magnetic susceptibility curves for samples **1c–d** (GAS samples) were obtained and studied. For each sample, the two peaks in  $\chi_M''$ , associated with the presence of the fast and slow relaxing species, are also observed. However, a deeper analysis and comparison of the  $\chi_M''$  curves for samples **1b–d** reveals variations in the ratio of both species and considerable temperature shifts of the maximum of the ac peaks. Moreover, considerable differences in  $U_{\text{eff}}$  for the slow relaxing species were observed. These effective energy barriers were found to be 63.7 K and 63.1 K for **1c** and **1d**, respectively, differing by almost 5 K with respect

**Table 2** Effective energy barriers ( $U_{\text{eff}}$ ) and pre-exponential factors ( $\tau_0$ ) obtained from the fit of the magnetic data to the Arrhenius law

Exp	Slow relaxing species		Fast relaxing species	
	$U_{\text{eff}}/\text{K}$	$\tau_0$	$U_{\text{eff}}/\text{K}$	$\tau_0$
<b>1a</b>	65.1	$4.2 \times 10^{-9}$	38.4	$1.5 \times 10^{-10}$
<b>1b</b>	66.7	$3.1 \times 10^{-9}$	36.1	$1.0 \times 10^{-10}$
<b>1c</b>	63.7	$6.9 \times 10^{-9}$	—	—
<b>1d</b>	63.1	$5.1 \times 10^{-9}$	—	—
<b>1e</b>	65.4	$3.4 \times 10^{-9}$	37.9	$3.1 \times 10^{-11}$
<b>1f</b>	64.2	$3.5 \times 10^{-9}$	37.0	$5.1 \times 10^{-11}$
<b>1h</b>	60.5	$6.3 \times 10^{-9}$	39.5	$6.8 \times 10^{-11}$
<b>1i</b>	58.6	$6.2 \times 10^{-9}$	37.7	$9.0 \times 10^{-11}$

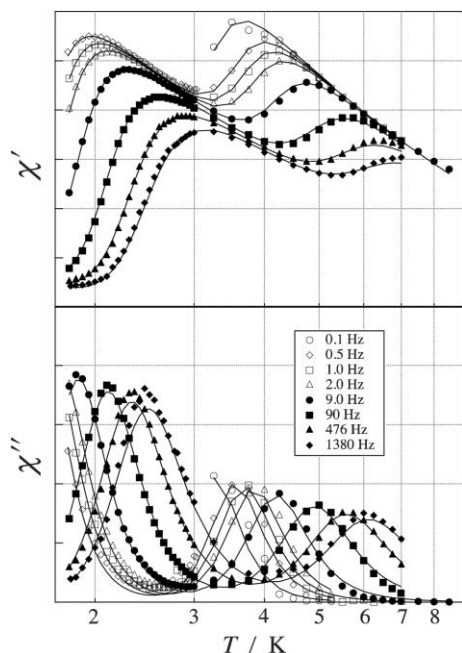


**Fig. 6** Ac magnetic susceptibilities of sample **1e**. Solid curves are best fits to the two-step Cole-Cole relaxation model.

to that found for sample **1b** (66.7 K).<sup>25</sup> This fact, together with the apparent changes in the proportions of the fast and slow relaxing species, reflect a clear influence of the particle size on the magnetization relaxation of the Mn<sub>12</sub> clusters.

Similar effects were observed for the ac magnetic susceptibilities of the ASES samples **1e**, **1f**, **1h**, and **1i**. As an example, a result of nonlinear least-squares fitting is shown in Fig. 6, where all the data were simultaneously used to provide a set of model parameters for sample **1e**. Effective energy barriers  $U_{\text{eff}}$  appear to be 65.4, 64.2, 60.5, and 58.6 K for slow-relaxing species and 37.9, 37.0, 39.5, 37.7 K for fast-relaxing species in samples **1e**, **1f**, **1h**, and **1i**, respectively. These values reveal a clear tendency in this case for the slow-relaxing magnetic species to show a lower energy barrier in a smaller microcrystal.

Finally, it is also remarkable that the reproducibility of the results obtained with both the GAS and ASES methods indicates that the variation dependence of the energy barrier is due to variations in the particle size rather than accuracy errors in the temperature range studied.

## Conclusions

Here we have reported for the first time the use of the Gas Anti-Solvent (GAS) and the Aerosol Solvent Extraction System (ASES) crystallization techniques, which use compressed CO<sub>2</sub> as an anti-solvent, for the crystallization of the SMM [Mn<sub>12</sub>O<sub>12</sub>(O<sub>2</sub>C<sub>6</sub>H<sub>5</sub>)<sub>16</sub>(H<sub>2</sub>O)<sub>4</sub>] (**1**). These studies have allowed us to: i) prepare crystalline samples of complex **1** with polymorphic purity, controlled particle size and narrower size distribution and ii) establish the influence of the particle size on the magnetization relaxation rates. Considering that samples **1b–i** obtained with these techniques have been shown

to exhibit the same crystallographic phase by XRPD data, the differences in their effective energy barriers most likely arise from: i) changes in the morphology along the miniaturization process, ii) variations in the molecular anisotropy (variations of the  $D$  value), iii) modifications in the tunnelling behaviour along the miniaturization process and iv) a combination of these factors. Further work is currently under way to shed more light on the origin of these differences, due to its importance for understanding the magnetization relaxation of SMMs and their potential technological implications. Finally, this experimental approach can be extended to the crystallization of several other functional magnetic molecular materials where control of a given property is highly desired.

## Acknowledgements

This work was supported by DGI (Spain) under projects MAT2002-0043 and MAT2003-04699 and by the European Commission under the NoE MAGMANET (Contract NMP3-CT-2005-515767) and QUEMOLNA Marie Curie RTN (Contract MRTN-CT-2003-5044880). The authors wish to thank MATGAS for the equipment and practical assessment in the high pressure experiments. Javier Campo and Nora Ventosa thank the Ramon y Cajal Program of Ministerio de Educación y Tecnología (Spain) for their contracts. Maria Muntó thanks the Consejo Superior de Investigaciones Científicas (CSIC) for her PhD bursary and Jordi Gómez-Segura thanks the European Community for his PhD grant.

## References

- (a) G. Christou, D. Gatteschi, D. N. Hendrickson and R. Sessoli, *MRS Bull.*, 2000, **25**, 56; (b) D. Gatteschi and R. Sessoli, *Angew. Chem., Int. Ed.*, 2003, **42**, 268.
- (a) R. Sessoli, D. Gatteschi, A. Caneschi and A. Novak, *Nature*, 1993, **365**, 141; (b) D. Gatteschi, A. Caneschi, L. Pardi and R. Sessoli, *Science*, 1994, **265**, 1054.
- (a) J. R. Friedman, M. P. Sarachik, J. Tejada and R. Ziolo, *Phys. Rev. Lett.*, 1996, **76**, 3830; (b) J. M. Hernández, X. X. Zhang, F. Luis, J. Bartolomé, J. Tejada and R. Ziolo, *Europhys. Lett.*, 1996, **35**, 301; (c) L. Thomas, F. Lioni, R. Ballou, D. Gatteschi, R. Sessoli and B. Barbara, *Nature*, 1996, **383**, 145.
- J. M. Hernandez, F. Torres, J. Tejada and E. Molins, *Phys. Rev. B: Condens. Matter Mater. Phys.*, 2002, **16**, 1407.
- (a) D. Ruiz-Molina, G. Christou and D. N. Hendrickson, *Mol. Cryst. Liq. Cryst.*, 2000, **343**, 335; (b) D. Ruiz, Z. S. Sun, B. Albelá, K. Folting, J. Ribas, G. Christou and D. N. Hendrickson, *Angew. Chem., Int. Ed.*, 1998, **37**, 300; (c) Z. M. Sun, D. Ruiz, E. Rumberger, C. D. Incarvito, K. Folting, A. L. Rheingold, G. Christou and D. N. Hendrickson, *Inorg. Chem.*, 1998, **37**, 4758.
- M. Soler, W. Wernsdorfer, Z. M. Sun, J. C. Huffman, D. N. Hendrickson and G. Christou, *Chem. Commun.*, 2003, 2672.
- Supercritical Fluid Technology in Material Science and Engineering*, ed. Y.-P. Sun, Marcel-Dekker, New York, 2002.
- C. F. Kirby and M. A. McHugh, *Chem. Rev.*, 1999, 99.
- J. M. DeSimone, *Science*, 2002, **297**, 799.
- A. I. Cooper, *Adv. Mater.*, 2003, **15**, 1049.
- J. D. Holmes, D. M. Lyons and K. J. Ziegler, *Chem.–Eur. J.*, 2003, **9**, 2144.
- H. M. Woods, M. M. C. G. Silva, C. Nouvel, K. M. Shakesheff and S. M. Howdle, *J. Mater. Chem.*, 2004, **14**, 1663.
- K. P. Johnston, *Science*, 2004, **303**, 482.
- J. J. Watkins and D. J. Bishop, *MRS Bull.*, 2004, **30**, 937.
- J. Jung and M. Perrut, *J. Supercrit. Fluids*, 2001, **20**, 179.
- D. W. Matson, J. L. Fulton, R. C. Petersen and R. D. Smith, *Ind. Eng. Chem. Res.*, 1987, **26**, 2298.

- 17 R. Thiering, F. Dehgani and N. R. Foster, *J. Supercrit. Fluids*, 2001, **21**, 159.
- 18 (a) N. Ventosa, S. Sala, J. Veciana, J. Llibre and J. Torres, *Cryst. Growth Des.*, 2001, **1**, 299; (b) N. Ventosa, S. Sala and J. Veciana, *J. Supercrit. Fluids*, 2003, **26**, 33.
- 19 E. Weidner, Z. Knez and Z. Novak, PGSS (Particles from gas saturated solutions) a new process for powder generation, in *Proceedings of the third International Symposium on Supercritical Fluids*, ed. G. Brunner and M. Perrut, I.S.A.S.F., Nancy (France), vol. 3, 1994, p. 229.
- 20 P. M. Gallagher, M. P. Coffey, V. J. Krukoni and N. Klasutis, Gas antisolvent recrystallization, new process to recrystallize compounds insoluble in supercritical fluids, *ACS Symp. Ser.*, 1989, **406**, 334.
- 21 J. Bleich, B. W. Müller and W. Wabmus, Aerosol solvent extraction system-a new microparticle production technique, *Int. J. Pharm.*, 1993, **97**, 111.
- 22 R. Sessoli, H.-L. Tsai, A. R. Schake, S. Wang, J. B. Vincent, K. Folting, D. Gatteschi and D. N. Hendrickson, *J. Am. Chem. Soc.*, 1993, **115**, 1805.
- 23 M. Gimeno, N. Ventosa, J. Veciana, Y. Boumghar, J. Fourier and I. Boucher, *J. Supercrit. Fluids*, 2005, DOI: 10.1016/j.supflu.2005.11.009.
- 24 A. M. Scurto, C. M. Lubbers, G. Xu and J. F. Brennecke, *Fluid Phase Equilib.*, 2001, **190**, 135.
- 25 In the same frequency range the  $\chi_M''$  peaks for **1c-d** appear out of the temperature working range. This was further evidence for the particle size influence on the magnetization relaxation of Mn<sub>12</sub> SMMs.

# Chemical Technology

A well-received news supplement showcasing the latest developments in applied and technological aspects of the chemical sciences



Free online and in print issues of selected RSC journals!\*

- **Application Highlights** – newsworthy articles and significant technological advances
- **Essential Elements** – latest developments from RSC publications
- **Free access** to the original research paper from every online article

\*A separately issued print subscription is also available

RSC Publishing

[www.rsc.org/chemicaltechnology](http://www.rsc.org/chemicaltechnology)

03005020